

BRepFormer: Transformer-Based B-rep Geometric Feature Recognition

Yongkang Dai
School of Software,
Northwestern Polytechnical
University
Xi'an, China
daiyongkang@mail.nwpu.edu.cn

Xiaoshui Huang
School of Public Health,
Shanghai Jiaotong
University
Shang hai, China
huangxiaoshui@163.com

Yunpeng Bai
School of Computing,
National University of
Singapore
Singapore
bai_yunpeng99@u.nus.edu

Hao Guo
School of Software,
Northwestern Polytechnical
University
Xi'an, China
guoh0215@mail.nwpu.edu.cn

Hongping Gan
School of Software,
Northwestern Polytechnical
University
Xi'an, China
ganhongping@nwpu.edu.cn

Ling Yang
Hangzhou Global Science and
Technology Innovation Center,
Zhejiang University
Hang zhou, China
3110101176@zju.edu.cn

Yilei Shi*
School of Software,
Northwestern Polytechnical
University
Xi'an, China
yilei_shi@nwpu.edu.cn

Abstract

Recognizing geometric features on B-rep models is a cornerstone technique for multimedia content-based retrieval and has been widely applied in intelligent manufacturing. However, previous research often merely focused on Machining Feature Recognition (MFR), falling short in effectively capturing the intricate topological and geometric characteristics of complex geometry features. In this paper, we propose BRepFormer, a novel transformer-based model to recognize both machining feature and complex CAD models' features. BRepFormer encodes and fuses the geometric and topological features of the models. Afterwards, BRepFormer utilizes a transformer architecture for feature propagation and a recognition head to identify geometry features. During each iteration of the transformer, we incorporate a bias that combines edge features and topology features to reinforce geometric constraints on each face. In addition, we also proposed a dataset named Complex B-rep Feature Dataset (CBF), comprising 20,000 B-rep models. By covering more complex B-rep models, it is better aligned with industrial applications. The experimental results demonstrate that

BRepFormer achieves state-of-the-art accuracy on the MFInstSeg, MFTRCAD, and our CBF datasets.

CCS Concepts

• **Computing methodologies** → **Computer vision problems**; *Shape modeling*; • **Applied computing** → *Computer-aided manufacturing*.

Keywords

CAD, Geometric Feature Recognition, Boundary Representation (B-rep), Transformer

ACM Reference Format:

Yongkang Dai, Xiaoshui Huang, Yunpeng Bai, Hao Guo, Hongping Gan, Ling Yang, and Yilei Shi. 2025. BRepFormer: Transformer-Based B-rep Geometric Feature Recognition. In *Proceedings of the 2025 International Conference on Multimedia Retrieval (ICMR '25), June 30-July 3, 2025, Chicago, IL, USA*. ACM, New York, NY, USA, 9 pages. <https://doi.org/10.1145/3731715.3733283>

1 Introduction

Geometric feature recognition serves as a critical link between Computer-Aided Design (CAD) and Computer-Aided Manufacturing (CAM). It is a cornerstone technique for multimedia content-based retrieval and plays a key role in automating manufacturing processes, improving efficiency, and reducing human errors. While traditional rule-based geometric feature recognition methods are widely used in industry, they are labor-intensive and struggle to adapt to complex geometric variations and topological changes [13, 18, 32]. To address these limitations, learning-based approaches have been introduced, often converting CAD models into intermediate representations such as point clouds [22], voxels [26], or images

*The corresponding author.

Permission to make digital or hard copies of all or part of this work for personal or classroom use is granted without fee provided that copies are not made or distributed for profit or commercial advantage and that copies bear this notice and the full citation on the first page. Copyrights for components of this work owned by others than the author(s) must be honored. Abstracting with credit is permitted. To copy otherwise, or republish, to post on servers or to redistribute to lists, requires prior specific permission and/or a fee. Request permissions from permissions@acm.org.

ICMR '25, Chicago, IL, USA

© 2025 Copyright held by the owner/author(s). Publication rights licensed to ACM.
ACM ISBN 979-8-4007-1877-9/2025/06
<https://doi.org/10.1145/3731715.3733283>

[31]. However, these transformations lead to key topological and geometric information loss, increased computational costs, and reduced recognition accuracy. Although recent deep learning models that directly process boundary representation (B-rep) data have shown promise in preserving geometric and topological details, as well as improving recognition accuracy [4], challenges remain in handling highly complex topologies and diverse manufacturing processes, limiting their practical effectiveness.

We propose BRepFormer, a transformer-based geometric feature recognition network that leverages a transformer architecture to effectively capture and process B-rep features. Unlike previous approaches that suffer from information loss and limited topological awareness [25], BRepFormer directly operates on the B-rep, ensuring high-fidelity feature extraction. Specifically, our model extracts both the geometric and topological features of the CAD model from multiple perspectives. During the feature encoding stage, geometric edge features and topological features are processed by separate encoders and then fused to form an attention bias, which serves as a constraint input into the transformer module. Meanwhile, the extracted geometric face features are encoded into tokens together with a virtual face. These tokens serve as carriers of information that are fed into the transformer module, facilitating deep interaction and information fusion among the features. Finally, the recognition head accepts the output from the transformer module and fuses the global and local features within it, achieving high-precision recognition of geometric features. By integrating these components, BRepFormer effectively propagates information across the CAD model structure, improving geometric feature recognition accuracy while preserving critical geometric and topological relationships.

We conducted experiments on the public MFInstSeg [35] and MFTRCAD [36] datasets, as well as our CBF dataset. The results demonstrate that BRepFormer achieves state-of-the-art recognition accuracy on these three datasets. Notably, BRepFormer excels in recognizing complex geometric structures and diverse machining features. On the MFTRCAD [36] dataset, it achieved a 93.16% recognition accuracy, surpassing the previous best method by 3.28 percentage points. To further validate the effectiveness of our approach, we performed detailed ablation studies, analyzing the impact of each model component on overall performance. The results show that every feature component helps boost the model's accuracy.

In summary, our proposed network, BRepFormer, effectively leverages the inherent information within the B-rep structure and achieves high-precision geometric feature recognition performance. The key contributions of this work are as follows:

- We develop a method (Sec. 3.2 and 3.3) that effectively extracts and encodes both topological and geometric features from CAD models, enabling a more informative and structured representation for machine learning models.
- We introduce a novel transformer-based architecture (Sec. 3.4) that enforces edge and face constraints during information propagation, significantly improving feature recognition accuracy.
- We introduce a CAD dataset (Sec. 4) that is more aligned with industrial applications, offering a more complex collection of CAD models to contribute to the geometric feature recognition.

- Our BRepFormer model achieves state-of-the-art accuracy on the experimental datasets, demonstrating the superiority of our approach.

2 Related Work

2.1 Rule-Based Geometric Feature Recognition

Rule-based geometric feature recognition methods identify geometric features in CAD models by applying predefined rules based on topological and geometric information. Early studies by Henderson [12], Donaldson [7], and Chan [5] introduced rule-based approaches that define boundary patterns and use expert systems for feature recognition. However, these methods lack flexibility due to the limitations of predefined rules, making it difficult to encode all machining knowledge and adapt to complex features.

Volumetric decomposition is another well-established rule-based approach for geometric feature recognition. This method decomposes the material to be removed from a CAD model into intermediate volumes and reconstructs geometric features based on predefined rules. Woo et al. [34] introduced the Alternating Sum of Volumes (ASV) method, representing solids as hierarchical convex bodies. Requicha et al. [32] further developed this approach to decompose machinable volumes into manufacturable features, addressing interactions through generation-testing strategies. Wilde et al. [19] refined the ASV method by introducing partitioning techniques to enhance its applicability.

Graph-based methods have gained attention due to their alignment with the B-rep structure of CAD models. These methods construct an Attribute Adjacency Graph (AAG) to capture topological and geometric information, and identify features by detecting subgraph patterns. Joshi et al. [18] first applied the AAG for topological and geometric information matching. Shah et al. [9] enhanced this approach by integrating hint-based feature recognition, introducing minimal condition subgraphs to improve the handling of feature interactions.

Hint-based methods [11, 24] use rules to identify complex intersecting features by extracting patterns and heuristic "hints" from residuals left by feature intersections. These hints guide the reconstruction of incomplete feature information through reasoning. While this method improves the recognition of intersecting features and aids subsequent process planning, defining comprehensive and precise hints, along with robust reasoning rules, remains challenging. This complexity makes the hint-based method challenging to achieve fully automated and high-precision feature recognition in practical applications.

2.2 Deep Learning-Based Geometric Feature Recognition

Various deep learning-based methods [14, 15, 22, 38, 40] have been developed for 3D structural representation, each addressing different challenges. Point-cloud-based methods leverage neural networks to extract features but often suffer from information loss. MFPointNet [22] employs selective downsampling layers for feature recognition, while Yao et al. [40] proposed a hierarchical neural network to improve the recognition of complex overlapping features. Shi et al. [30] introduced a multi-sectional view (MSV)

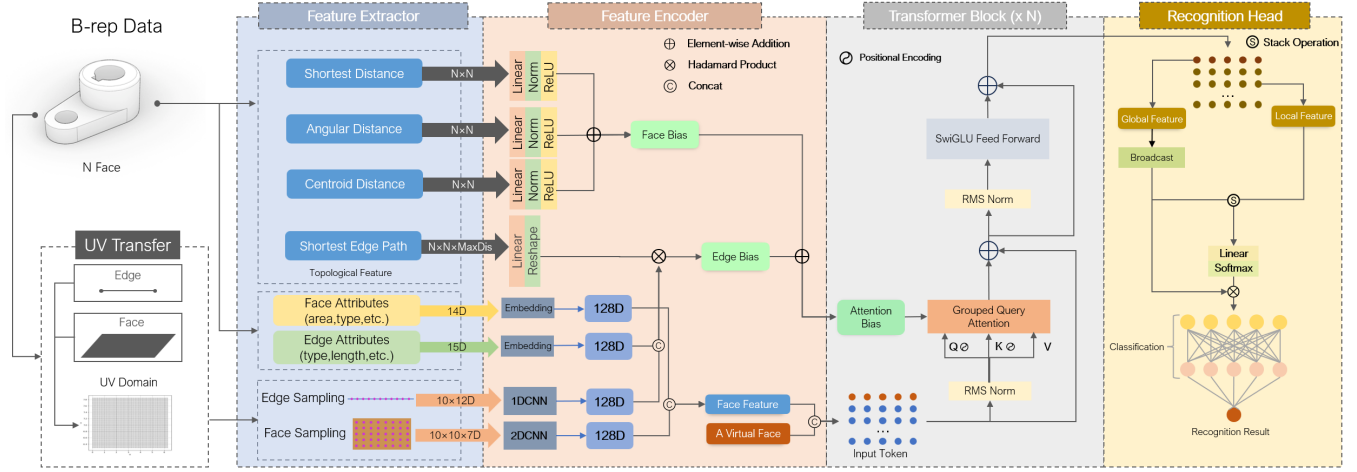


Figure 1: Our model consists of four main components: (1) Feature Extractor, which extracts topological and geometrical features from the B-rep model; (2) Feature Encoder, where edge and topological features are combined to create an attention bias and face features are augmented with a virtual face before being input into the transformer block; (3) Transformer Block, which processes the encoded features using grouped query attention and attention bias; and (4) Recognition Head, where the output features are fused and passed through a classification head to obtain the recognition results.

representation and MsvNet, enriching 3D model representation by incorporating multi-view features.

Voxel-based approaches use 3D CNNs to process CAD models but suffer from resolution-related information loss. For example, FeatureNet [42] applies 3D CNNs for feature recognition, and Pedireddy et al. [27, 28] refined voxelization techniques to predict machining processes like milling and turning. However, voxelization inherently reduces geometric fidelity, especially at low resolutions. Mesh-based methods aim to retain geometric details for better recognition. Jia et al. [17] proposed a method combining MeshCNN with Faster RCNN (Mesh Faster RCNN) to enhance detection accuracy while preserving mesh geometry. However, the high memory demand for processing high-resolution data limits its scalability in large-scale scenarios.

In the CAD industry, B-rep is the dominant format for 3D models, making graph-based representations particularly effective. Graph neural networks (GNNs) have been widely applied due to their structural similarity with B-rep. For example, Cao et al. [4] pioneered the transformation of B-rep models into graph-structured representations for learning. Colligan et al. [6] introduced Hierarchical CADNet, a novel approach that leverages a two-level graph representation to improve recognition accuracy. Specifically, it utilizes the Face Adjacency Graph (FAG) to capture topological information and mesh patches to represent geometric details. Jayaraman et al. [16] proposed UV-Net, which encodes surfaces and curves with CNNs and utilizes graph convolutional networks (GCNs) for feature learning.

Recent advancements further refine B-rep-based learning methods. Lambourne et al. [20] developed BRepNet, which defines convolution kernels for directed coedges, improving pattern detection. Lee et al. [21] introduced BRepGAT, incorporating graph attention networks (GATs) for precise feature segmentation. Wu et al.

[35] proposed AAGNet, a multi-task GNN that simultaneously performs semantic, instance, and base segmentation using the geometric attribute adjacency graph (gAAG). Xia et al. [36] developed MFTReNet, which learns semantic segmentation, instance grouping, and topological relationship prediction directly from B-rep data. Despite these advancements, the generation of large-scale datasets with detailed topological labels requires substantial annotation efforts, thereby increasing the cost of data preparation.

3 Method

3.1 Overview

We propose a novel approach for CAD geometric feature recognition based on a transformer architecture as shown in Figure 1, consisting of four different parts: 1) **Feature Extractor Module** considers the topological and geometric features of the model from multiple perspectives; 2) **Feature Encoder Module** encodes the initial input features into a format that is friendly for the network, thereby generating the main integrated features; 3) **Transformer Block Module** further extracts features using a transformer structure, with a designed attention bias constraint; 4) **Recognition Head Module** fuses the features and classifies the faces of B-rep data.

3.2 Feature Extraction Module

The Feature Extraction Module extracts feature for both the geometry and topology of the B-rep model, focusing on faces and edges.

3.2.1 Topological Feature Extraction. For topology, we extract four different features, including three face features (Face Shortest Distance, Face Angular Distance and Face Centroid Distance) and one feature for edges (Shortest Edge Path).

Face Shortest Distance. To fully capture the direct and indirect spatial relationships between any two faces in the B-rep model, we employed the Dijkstra algorithm to compute the shortest path length between all pairs of faces. This method quantifies the topological distance between faces as the number of intervening faces along the connecting path. Based on these results, we constructed an extended adjacency matrix $M_d \in \mathbb{R}^{N \times N}$, where each element $m_d(f_i, f_j)$ represents the shortest distance from any face f_i to another face f_j . This matrix captures not only direct connections between faces but also indirect connections via other faces, thereby reflecting complex connectivity patterns.

Face Angular Distance. To accurately describe the relative position between two faces, our approach extracts the dihedral angle between them. For adjacent faces sharing a common edge, the dihedral angle indicates their geometric relationship (e.g., concave, convex, or smooth transition). For non-adjacent faces, we calculate the angle between their normal vectors, reflecting their relative orientation in 3D space regardless of intermediate faces. At the same time, our approach also constructs a matrix $M_a \in \mathbb{R}^{N \times N}$ to represent the angular information between faces, where each element $m_a(f_i, f_j)$ represents the angle between a face f_i and another face f_j .

Face Centroid Distance. The centroid distance between faces, a key topological feature, quantifies their spatial separation by measuring the Euclidean distance between face centroids. To eliminate scale influence, we normalize this distance by the bounding box diagonal length of the solid model, yielding a relative distance indicator. This normalized distance reflects similarity between CAD models of varying sizes and proportions. Similarly, we construct a matrix $M_c \in \mathbb{R}^{N \times N}$ to represent the angular information between faces, where each element $m_c(f_i, f_j)$ represents the Euclidean distance between the centroids of face f_i and face f_j .

Shortest Edge Path. Considering the key role of edges in defining global topological features, our approach particularly focuses on the shortest edge path between any two faces. Edges are not only the basic elements connecting different faces but also carry rich information about the model’s internal connectivity and surface continuity. Therefore, for any two face f_i and f_j in the B-rep model, we not only calculate the shortest distance between them but also record all the edge chains $\{e_{ik}, e_{kl}, \dots, e_{mj}\}$ that make up this shortest path. To effectively represent this edge path information, we introduce a three-dimensional matrix $M_e \in \mathbb{R}^{N \times N \times \text{MaxDistance}}$ to store edge path data. The parameter MaxDistance is employed to specify the upper limit of the distance between any two surfaces within a single model. For any pair of surfaces (f_i, f_j) , in a given model, when the shortest path distance between them is less than MaxDistance, the elements in the edge path matrix that exceed the actual shortest path range will be initialized to -1 as an indicator of invalid values.

3.2.2 Geometric Feature Extraction. Our approach further conducts geometric feature extraction from two aspects: the UV domain and geometric attributes, as detailed below.

For extracting UV domain features from CAD models, we follow a method inspired by UV-Net [16]. We sample and discretize the parametric surfaces and parametric curves surfaces in B-rep into regular 2D and 1D point grids with a uniform step size, as shown in

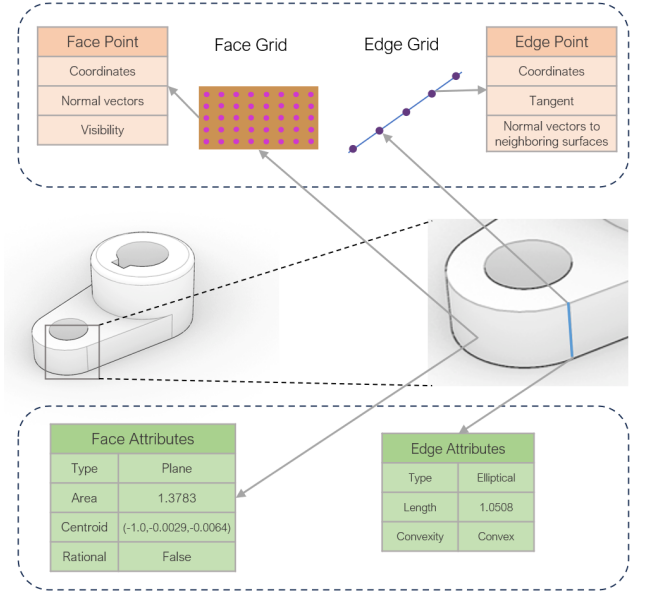


Figure 2: The upper part of the figure shows the details of geometric UV domain sampling, while the lower part shows the details of geometric attribute sampling.

Figure 2. Each face’s grid includes 3D coordinates, normal vectors of the points, and a visibility indicator. Each edge’s grid includes 3D coordinates, tangent vectors, and the normal vectors of the adjacent faces. Compared to discrete methods like voxel grids [39] and traditional meshes [8], our UV grids capture precise geometric details and provide a suitable input format for neural networks.

Furthermore, our method also extracts the geometric attributes inherent in the solid entities of CAD models as show in Figure 2. To characterize the geometric attribute features of surfaces, we extract the following information: surface type (e.g., plane, conical surface, cylindrical surface, etc.), area, centroid coordinates, and whether it is a rational B-spline surface. For the geometric attribute features of curved edges, we extract their type (e.g., circular, closed curve, elliptical, straight line, etc.), length, and convexity (i.e., concave, convex, or smooth transition). These geometric attributes of faces and edges can be directly obtained from the original B-rep structure and are encoded separately. By integrating the aforementioned geometric attributes extracted from the UV domain, we obtain a geometric input representation of the entire CAD model, which provides strong support for subsequent downstream tasks.

3.3 Feature Encoder Module

Feature encoder module further encodes all features extracted above, and output an attention bias and faces features, as the input for the following module.

3.3.1 Topological Feature Encoder. For the above-mentioned three topological relation matrices $M_d, M_a, M_c \in \mathbb{R}^{N \times N}$ between faces, we applied a unified processing pipeline to these matrices. Specifically, each matrix is first transformed through a linear layer of the same dimension, followed by sequential processing through

Table 1: Geometric Feature Dimensions in UV Domain

Element	Feature	Dimension
Face	Coordinates	3D
	Normal vectors	3D
	Visibility	1D
Edge	Coordinates	3D
	Tangent	3D
	Normal vectors to neighboring surfaces	6D

a normalization layer and a ReLU activation function for feature encoding, which is formulated as:

$$M'_i = \text{ReLU}(\text{Norm}(\text{Linear}(M_i))) \quad (1)$$

here, M_i denotes the three topological matrices M_d , M_a , and M_c .

Based on these three parts, we obtain the face bias input into the transformer module:

$$B_{\text{Face}} = \text{Add}(M'_d, M'_a, M'_c) \quad (2)$$

within the framework of the edge path matrix, we have considered the impact of edge weights on faces. For the shortest path between any two faces in a B-rep model, the influence of distant edges on the initial face diminishes progressively as the position along the path advances from the starting face. Based on these considerations, our method integrates the edge path matrix with edge features to model the weight influence of edges on faces along the path. The formula is expressed as follows:

$$B_{\text{Edge}} = (M_e \otimes H_{\text{edge}}) \quad (3)$$

here, M_e stands for the edge path matrix, and H_{edge} indicates the extracted and encoded edge features.

Finally, the sum of the obtained B_{Edge} and B_{Face} yields the attention bias that we input into the transformer module as shown in Figure 1.

3.3.2 Geometric Feature Encoder. For the encoding of UV domain sampling features in CAD geometric features, BRepFormer encodes face feature as $f_{\text{geo}} \in \mathbb{R}^{N_f \times N_u \times N_v \times 7}$, and edge feature as $e_{\text{geo}} \in \mathbb{R}^{N_e \times N_u \times 12}$. Here, N_f and N_v indicate the number of sampling points for faces and edges based on the UV grid parameters respectively. N_u and N_v represent the number of sampling points along the u-axis and v-axis. The aforementioned geometric features are all fed into their respective encoders. The face encoder consists of three 2D CNN layers, an adaptive average pooling layer, and a fully connected layer, which encode the face features into a feature dimension of 128. Similarly, the edge encoder has a structure akin to the face encoder but uses 1D CNN layers for preliminary encoding. The encoded information of geometric features is shown in Table 1.

We employed Multilayer Perceptrons (MLP) to encode the geometric attribute features of faces and edges. The encoded face attributes include a 9-dimensional one-hot vector $f_{\text{type}} \in \mathbb{R}^9$ to represent surface types (e.g., plane, conical surface, cylindrical surface, etc.), a vector $f_{\text{area}} \in \mathbb{R}^1$ to identify the surface area, a vector $f_{\text{cen}} \in \mathbb{R}^3$ to identify the centroid coordinates of the face, and a

Table 2: Attribute Feature Encoding for Geometric Elements

Element	Input Feature	Encoder Layer	Output
Face	$f_{\text{type}} \in \mathbb{R}^9$	Linear (9, 32)	$h_{f,\text{type}} \in \mathbb{R}^{32}$
	$f_{\text{area}} \in \mathbb{R}^1$	Linear (1, 32)	$h_{f,\text{area}} \in \mathbb{R}^{32}$
	$f_{\text{cen}} \in \mathbb{R}^3$	Linear (3, 32)	$h_{f,\text{cen}} \in \mathbb{R}^{32}$
Edge	$f_{\text{rat}} \in \mathbb{R}^1$	Linear (1, 32)	$h_{f,\text{rat}} \in \mathbb{R}^{32}$
	$e_{\text{type}} \in \mathbb{R}^{11}$	Linear (11, 64)	$h_{e,\text{type}} \in \mathbb{R}^{64}$
	$e_{\text{len}} \in \mathbb{R}^1$	Linear (1, 32)	$h_{e,\text{len}} \in \mathbb{R}^{32}$
	$e_{\text{conv}} \in \mathbb{R}^3$	Linear (3, 32)	$h_{e,\text{conv}} \in \mathbb{R}^{32}$

vector $f_{\text{rat}} \in \mathbb{R}^1$ to identify whether it is a rational B-spline surface. The edge attributes include an 11-dimensional one-hot vector $e_{\text{type}} \in \mathbb{R}^{11}$ for identifying edge types (e.g., circular, closed curve, elliptical, straight line, etc.), a vector $e_{\text{len}} \in \mathbb{R}^1$ to identify the type of the edge, and a 3-dimensional one-hot vector $e_{\text{conv}} \in \mathbb{R}^3$ to characterize the convexity of the edge (concave, convex, or smooth). The encoded information of attribute features is shown in Table 2 as indicated.

Finally, by concatenating the encoded features of the two types of geometric attributes and the geometric UV domain features, we obtained the complete geometric face and edge features, H_{face} and H_{edge} respectively:

$$H_{\text{face}} = \text{Concat}(h_{f,\text{geo}}, h_{f,\text{type}}, h_{f,\text{area}}, h_{f,\text{cen}}, h_{f,\text{rat}}) \in \mathbb{R}^{256} \quad (4)$$

$$H_{\text{edge}} = \text{Concat}(h_{e,\text{geo}}, h_{e,\text{type}}, h_{e,\text{len}}, h_{e,\text{conv}}) \in \mathbb{R}^{256} \quad (5)$$

3.4 Transformer Block Module

Before feeding the encoded face features into our transformer architecture, we introduced a virtual face feature that is connected to all B-rep elements. This virtual face feature, within the transformer structure, can engage in deep interactions with the actual face features, thereby obtaining a global feature that represents the entire B-rep model.

This part consists of 8 layers of designed transformer modules, with each layer primarily incorporating Grouped Query Attention (GQA) [1], Root Mean Square Normalization (RMS Norm), and SwiGLU activation function. First, all the feature of the faces are represented as $H_{\text{face}}^0 = [h_{\text{face}}^1, h_{\text{face}}^2, \dots, h_{\text{face}}^{N+1}] \in \mathbb{R}^{(N+1) \times 256}$. Here, each h_{face}^i represents the feature of a given face, $N + 1$ indicates that it includes the features of the virtual face, and the superscript 0 in H_{face}^0 denotes the initial iteration of the overall feature representation.

First, all the input face features are fed into RMS Norm for normalization. Next, the normalized features are fed into the GQA for feature propagation. Following this, the features processed by the attention mechanism are fed into the Feed-Forward Network (FFN), and then combined with residual connections for further processing. The overall formula expressed as follows:

$$H_{\text{face}}^{t'} = \text{Attention} \left(\text{RMS Norm}(H_{\text{face}}^{t-1}) \right) + H_{\text{face}}^{t-1} \quad (6)$$

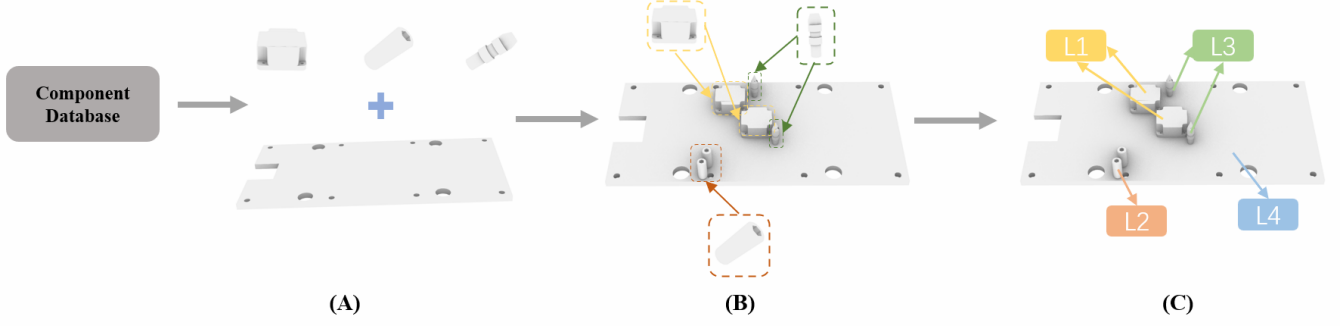


Figure 3: The entire process of constructing our dataset, (A) illustrates the selection of four components from the database, (B) shows the application of random rotation, translation, and duplication under geometric constraints to generate a new B-rep model, and (C) demonstrates the process of traversing and labeling all faces (L1, L2, L3, L4).

$$H_{\text{face}}^t = \text{FFN} \left(\text{RMS Norm}(H_{\text{face}}^t) \right) + H_{\text{face}}^t \quad (7)$$

Our attention uses GQA, which divides the queries into multiple groups and independently computes attention within each group. It then concatenates the outputs of all groups Q_g and passes them through a linear transformation to obtain the output, effectively reducing computational load and memory usage, and t indicates the iteration times. The specific expression formula for GQA is as follows:

$$O = \left(\text{Concat} \left[\text{softmax} \left(\frac{Q_g K^T}{\sqrt{d_k}} + B_{\text{Att}} \right) V \right]_{g=1}^G \right) W_o \quad (8)$$

where O refers to the final output, G indicates the upper limit of the number of groups. For each group g , the dot product of Q_g and K is first scaled by the square root of the key vector dimension d_k . This scaled product is then adjusted by the attention bias B_{Att} , and the softmax function is applied to obtain the attention weights. These weights are used to compute the weighted sum of the values V . The outputs of all groups are concatenated and passed through a linear transformation W_o to produce the final output O .

In the FFN layer, we primarily use the SwiGLU activation function, which is mathematically expressed as follows:

$$\text{SwiGLU} = \text{Swish}(Wx + b) \otimes (Vx + c) \quad (9)$$

here, W and V denote the learnable weight matrices that are applied to the input x , b and c are bias terms. The Swish activation function defined as $\text{Swish}(z) = z \cdot \text{sigmoid}(z)$.

Finally, based on the introduced global virtual face feature and the input encoded face features, the module outputs f_{global} , representing the global feature of the B-rep model, and f_{local} , representing the local feature.

3.5 Recognition Head

Based on the local feature representation of f_{local} and the global feature f_{global} output by the transformer module, we design a structure to fuse these two parts of features. First, we broadcast the global feature to the same dimension as the local feature and stack the two parts along a new dimension to obtain the integrated feature

representation F_{all} . Then, we multiply the features F_{all} by a learnable weight matrix W_w and apply a softmax activation function to obtain the weight representation of these features. Finally, we perform element-wise multiplication between this weight representation and the F_{all} to generate the final output features. The specific formulas are as follows:

$$F_{\text{all}} = \text{stack}[f_{\text{local}}, f_{\text{global}}] \quad (10)$$

$$F_{\text{out}} = F_{\text{all}} \otimes \text{softmax}(F_{\text{all}} \cdot W_w + b_w) \quad (11)$$

where stack denotes the operation of concatenation along a new dimension, F_{all} represents the newly obtained features, W_w represents the learnable weight matrix of the linear layer and b_w denotes the bias term associated with it.

For the final feature recognition task in CAD models, we employed a MLP coupled with an argmax activation function as the classifier to predict the geometric feature category \hat{C} of each face. The mathematical expression is as follows:

$$\hat{C} = \text{arg max}(\text{MLP}(F_{\text{out}})) \in \mathbb{R}^{N \times K} \quad (12)$$

We choose the cross-entropy as our final loss function, which is as follow:

$$L = -\frac{1}{N} \sum_{i=1}^N \sum_{j=1}^C y_{i,j} \log(\hat{C}_{i,j} + \epsilon) \quad (13)$$

here, ϵ is a small positive constant added to the predicted probabilities to ensure numerical stability

4 Complex B-rep Feature (CBF) Dataset

We introduce the CBF dataset to support research on complex geometric feature recognition. It contains 20,000 B-rep CAD models, each formed by combining a base plate with three geometric features. The faces of these features are labeled and stored in JSON files for model construction and training research.

For our data creation process, Figure 3 demonstrates the entire workflow. We first selected B-rep from public sources and separated the base plates and geometric features using relevant 3D modeling software. Subsequently, we applied random rotations, translations,

and duplications to the three extracted geometric features on the base plate. During these operations, we ensured the rationality of the generated models by manipulating their geometric constraints. Specifically, for translation, the script moved the model along the normal and tangent vectors of the contact surface until it intersected with the base plate, ensuring proper attachment. Rotations were performed based on the geometric attributes of the contact surface (such as normal vectors and centroids) to avoid model distortion or detachment. Duplication was carried out via boolean operations to ensure that the newly generated components did not conflict with the base plate or other components. Finally, in the labeling stage, we traversed all faces of the composite model, determined which original component each face belonged to (base plate, feature A, feature B, feature C), and assigned a label to each face. This information was stored in a dictionary, with face indices as keys and corresponding component labels as values.

5 Experiments

5.1 Experimental Environment

We trained our network using a single NVIDIA 4090 GPU and PyTorch-Lightning v1.9.0, highlighting its lightweight nature. During training, we used the AdamW optimizer with an initial learning rate of 0.001, and parameters set to $\beta_1 = 0.9$, $\beta_2 = 0.999$, and $\epsilon = 1 \times 10^{-8}$ for stability. We also employed the ReduceLROnPlateau [2] learning rate scheduler to dynamically adjust the learning rate based on validation loss. A linear learning rate warm-up was implemented for the first 5000 steps to aid convergence. The batch size was set to 64, and training lasted up to 200 epochs.

To evaluate the performance of our network, we used overall accuracy A , class accuracy A_c , and mean Intersection over Union (mIoU) to verify the performance of our model’s geometric feature recognition capabilities, mathematically expressed as follows:

$$A = \frac{F_c}{F_t} \quad (14)$$

here, F_c denotes the number of correctly classified B-rep faces, and F_t is the total number of B-rep faces in the CAD model. Overall accuracy A calculates the proportion of correctly classified B-rep faces to the total number of B-rep faces in the CAD model.

$$A_c = \frac{1}{C} \sum_{c=1}^C \frac{\hat{y}_c = l_c}{y_c = l_c} \quad (15)$$

here, A_c denotes the average accuracy across all classes. y_c represents the total number of B-rep faces in label l_c , while \hat{y}_c indicates the number of correctly predicted B-rep faces in label l_c . The class accuracy A_c represents the average accuracy across all geometric feature classes.

$$mIoU = \frac{1}{C} \sum_{c=1}^C \frac{\hat{y}_c = l_c \cap y_c = l_c}{\hat{y}_c = l_c \cup y_c = l_c} \quad (16)$$

here, the parameter expressions in this part are the same as those described above for A_c . The mIoU is commonly used to evaluate the overlap between predicted results and true labels. In the context of our geometric feature recognition task, mIoU is calculated as the average ratio of correctly classified B-rep faces that share the same class labels in both the actual and predicted outputs.

5.2 Experimental Datasets

We evaluated our model’s machining feature recognition ability on the MFInstSeg and MFTRCAD public datasets and compared it with mainstream deep learning methods. Our model achieved state-of-the-art accuracy on these datasets. We also tested its complex feature recognition capability on the proposed CBF dataset, where it again achieved state-of-the-art accuracy. For all datasets, we used a 70% / 15% / 15% split for training, validation, and testing.

5.2.1 MFInstSeg Dataset. The MFInstSeg dataset comprises 62,495 CAD model files stored in B-rep format. It includes 24 different types of machining features, with each model containing 3 to 10 unique machining features. Table 3 shows the performance of our model and other mainstream models on this dataset.

Table 3: Recognition Performance on MFInstSeg Dataset

Network	Accuracy(%)	mIoU(%)
ASIN[41]	86.46 ± 0.45	79.15 ± 0.82
GATv2[3]	95.90 ± 0.20	93.03 ± 0.36
GraphSAGE[10]	97.69 ± 0.06	95.70 ± 0.14
GIN[37]	98.14 ± 0.03	96.52 ± 0.06
DeeperGCN[23]	99.03 ± 0.02	98.31 ± 0.01
AAGNet[35]	99.15 ± 0.03	98.45 ± 0.04
MFTRNet[36]	99.56 ± 0.02	98.43 ± 0.03
BRepFormer(Ours)	99.62 ± 0.03	98.74 ± 0.09

5.2.2 MFTRCAD Dataset. The MFTRCAD dataset comprises 28,661 CAD models stored in B-rep format. The authors further divided one of the traditional 24 machining feature categories into three subcategories, leading to a total of 26 distinct machining features in the dataset. Table 4 presents the performance of our model and other mainstream models on this dataset.

Table 4: Recognition Performance on MFTRCAD Dataset

Network	Accuracy(%)
PointNet++[29]	67.89 ± 0.08
DGCNN[33]	67.97 ± 0.07
ASIN[41]	68.57 ± 0.41
Hierarchical CADNet[6]	78.39 ± 0.03
AAGNet[35]	79.45 ± 0.02
MFTRNet[36]	89.88 ± 0.02
BRepFormer(Ours)	93.16 ± 0.11

5.2.3 Complex Feature Dataset. In our CBF dataset, unlike previous datasets, this dataset requires the model to identify these three distinct geometric features along with the base plate. The experimental results of our model and other mainstream models on this dataset is presented in Table 5.

Although our network outperforms other comparative networks in terms of overall accuracy, it performs poorly in the mIoU metric. Analysis reveals that when the network identifies simple geometric features, the limited number of faces involved means that any misidentification significantly impacts overall accuracy. In contrast, when dealing with complex geometric features, the higher number

Table 5: Recognition Performance on CBF Dataset

Network	Accuracy(%)	Class Acc(%)	mIoU(%)
AAGNet[35]	93.41	-	93.76
MFTRNet[36]	92.12	-	91.21
BRepFormer(Ours)	94.66	94.97	87.48

of faces means that misidentification of some faces has a relatively limited impact on overall accuracy. Based on the above analysis, despite certain shortcomings in the mIoU metric, our network still maintains a leading position in overall recognition accuracy. This indicates that our network is more adept at recognizing complex, multi-faceted geometric features.

5.3 Ablation Study

In the ablation study, we focused on the impact of the input features of our model on its performance. We systematically removed these key features and tested the changes in model performance. All ablation experiments were conducted on our proposed CBF dataset.

5.3.1 Ablation Analysis of Geometric Features. In our ablation study, we tested the importance of different input features for the BRepFormer network. The network takes UV domain geometric features and B-rep attribute features as inputs. We compared a baseline model with complete inputs to models that removed each of these features individually. The results in Table 6 show that removing any input feature reduces feature recognition accuracy. Specifically, removing attribute features causes the most significant performance drop, while removing UV domain geometric features has a smaller impact. This indicates that attribute features are more critical than geometric features in our network architecture.

Table 6: Impact of Removing Different Geometric Features on BRepFormer Performance

Input	Accuracy(%)	Class Acc(%)	mIoU(%)
Full (baseline)	94.66	94.97	87.48
w/o Face Attr	92.34 (-2.32)	91.23 (-3.74)	84.10 (-3.38)
w/o Edge Attr	91.01 (-3.65)	90.01 (-4.96)	81.69 (-5.79)
w/o UV-grid	92.95 (-1.71)	91.85 (-3.12)	85.05 (-2.43)

5.3.2 Ablation Analysis of Topological Features. In our BRepFormer network, we focused on extracting four key topological features from CAD models to delineate the comprehensive relational structure of B-rep models. To demonstrate the effectiveness of the extracted features, we established a baseline model using the initial complete topological features and then conducted ablation experiments by progressively removing topological features on our CBF dataset. As shown in Table 7, the network’s accuracy decreased successively with the removal of each of the topological features. This indicates that the global topological matrices facilitate accurate understanding of complex 3D solid models by neural network.

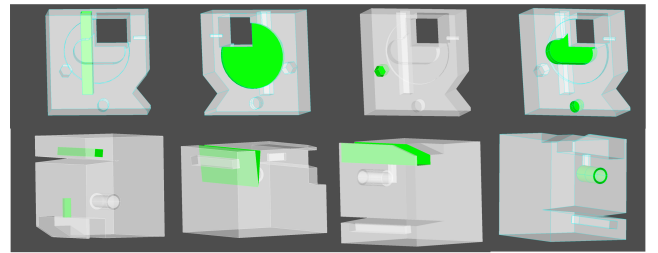
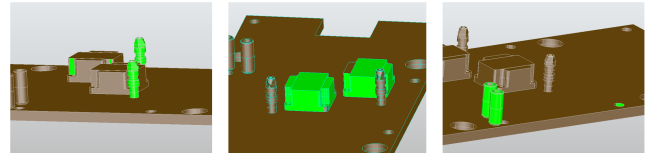
5.4 Geometric Recognition Presentation

This section presents a visual demonstration of our network’s performance in geometric feature recognition. Figure 4 illustrates the

Table 7: Impact of Removing Different Topological Features on BRepFormer Performance

Input	Accuracy(%)	Class Acc(%)	mIoU(%)
Full (baseline)	94.66	94.97	87.48
w/o M_d	93.51 (-1.15)	92.73 (-2.24)	86.28 (-1.20)
w/o M_d, M_a and M_c	93.33 (-1.33)	92.29 (-2.68)	85.95 (-1.53)
w/o M_d, M_a, M_c and M_e	93.22 (-1.44)	92.17 (-2.80)	85.60 (-1.88)

network’s capability in identifying machining features, with the green highlights indicating the features that have been successfully recognized by the network. Figure 5, meanwhile, displays the outcomes of our network’s feature recognition on more complex geometric shapes.

**Figure 4: Examples of recognized machining features (highlighted in green) in B-rep models****Figure 5: Examples of recognized complex features (highlighted in green) in B-rep models**

6 Conclusion

In this paper, we introduce BRepFormer, a novel geometric feature recognition network based on the transformer architecture. Our network effectively extracts both geometric and topological information from CAD models, and incorporates an attention bias that integrates geometric and topological features to regulate information propagation within the transformer module. Furthermore, we propose the CBF dataset, which features more complex geometric and topological representations and is specifically designed for complex feature recognition tasks. Finally, BRepFormer achieves state-of-the-art accuracy on the public MFInstSeg and MFTRCAD datasets, as well as our CBF dataset, thereby demonstrating its superiority in both machining feature recognition and complex geometric feature recognition tasks.

7 Acknowledgments

This research was funded by the Fundamental Research Funds for the Central Universities, the Natural Science Basic Research Program of Shaanxi Province under Grant 2024JC-YBQN-0702, and NUS Research Scholarship and NUS ORIA.

References

- [1] Joshua Ainslie, James Lee-Thorp, Michiel de Jong, Yury Zemlyanskiy, Federico Lebrón, and Sumit Sanghai. 2023. Gqa: Training generalized multi-query transformer models from multi-head checkpoints. *arXiv preprint arXiv:2305.13245* (2023).
- [2] Ayman Al-Kababji, Faycal Bensaali, and Sarada Prasad Dakua. 2022. Scheduling techniques for liver segmentation: Reducelronplateau vs onecyclelr. In *International conference on intelligent systems and pattern recognition*. Springer, 204–212.
- [3] Shaked Brody, Uri Alon, and Eran Yahav. 2021. How attentive are graph attention networks? *arXiv preprint arXiv:2105.14491* (2021).
- [4] Weijuan Cao, Trevor Robinson, Yang Hua, Flavien Boussuge, Andrew R Colligan, and Wanbin Pan. 2020. Graph representation of 3D CAD models for machining feature recognition with deep learning. In *International design engineering technical conferences and computers and information in engineering conference*, Vol. 84003. American Society of Mechanical Engineers, V11AT11A003.
- [5] AKW Chan and Keith Case. 1994. Process planning by recognizing and learning machining features. *International Journal of Computer Integrated Manufacturing* 7, 2 (1994), 77–99.
- [6] Andrew R Colligan, Trevor T Robinson, Declan C Nolan, Yang Hua, and Weijuan Cao. 2022. Hierarchical cadnet: Learning from b-reps for machining feature recognition. *Computer-Aided Design* 147 (2022), 103226.
- [7] Iain A Donaldson and Jonathan R Corney. 1993. Rule-based feature recognition for 2-5D machined components. *International Journal of Computer Integrated Manufacturing* 6, 1-2 (1993), 51–64.
- [8] Yutong Feng, Yifan Feng, Haoxuan You, Xibin Zhao, and Yue Gao. 2019. Meshnet: Mesh neural network for 3d shape representation. In *Proceedings of the AAAI conference on artificial intelligence*, Vol. 33. 8279–8286.
- [9] Shuming Gao and Jami J Shah. 1998. Automatic recognition of interacting machining features based on minimal condition subgraph. *Computer-Aided Design* 30, 9 (1998), 727–739.
- [10] Will Hamilton, Zhitao Ying, and Jure Leskovec. 2017. Inductive representation learning on large graphs. *Advances in neural information processing systems* 30 (2017).
- [11] JungHyun Han and Aristides AG Requicha. 1997. Integration of feature based design and feature recognition. *Computer-Aided Design* 29, 5 (1997), 393–403.
- [12] Mark Richard Henderson. 1984. *Extraction of feature information from three-dimensional CAD data*. Purdue University.
- [13] Mark R Henderson and David C Anderson. 1984. Computer recognition and extraction of form features: a CAD/CAM link. *Computers in industry* 5, 4 (1984), 329–339.
- [14] Xiaoshui Huang, Zhou Huang, Sheng Li, Wentao Qu, Tong He, Yuenan Hou, Yifan Zuo, and Wanli Ouyang. 2024. Frozen CLIP Transformer Is an Efficient Point Cloud Encoder. In *Proceedings of the AAAI Conference on Artificial Intelligence*, Vol. 38. 2382–2390.
- [15] Xiaoshui Huang, Zhou Huang, Yifan Zuo, Yongshun Gong, Chengdong Zhang, Deyang Liu, and Yuming Fang. 2025. PSReg: Prior-guided Sparse Mixture of Experts for Point Cloud Registration. *arXiv preprint arXiv:2501.07762* (2025).
- [16] Pradeep Kumar Jayaraman, Aditya Sanghi, Joseph G Lambourne, Karl DD Willis, Thomas Davies, Hooman Shayani, and Nigel Morris. 2021. Uv-net: Learning from boundary representations. In *Proceedings of the IEEE/CVF conference on computer vision and pattern recognition*. 11703–11712.
- [17] Jia-Le Jia, Sheng-Wen Zhang, You-Ren Cao, Xiao-Long Qi, and WeZhu. 2023. Machining feature recognition method based on improved mesh neural network. *Iranian Journal of Science and Technology, Transactions of Mechanical Engineering* 47, 4 (2023), 2045–2058.
- [18] Sanjay Joshi and Tien-Chien Chang. 1988. Graph-based heuristics for recognition of machined features from a 3D solid model. *Computer-aided design* 20, 2 (1988), 58–66.
- [19] Yong Se Kim and DJ Wilde. 1992. A convergent convex decomposition of polyhedral objects. (1992).
- [20] Joseph G Lambourne, Karl DD Willis, Pradeep Kumar Jayaraman, Aditya Sanghi, Peter Meltzer, and Hooman Shayani. 2021. Brepnet: A topological message passing system for solid models. In *Proceedings of the IEEE/CVF conference on computer vision and pattern recognition*. 12773–12782.
- [21] Jinwon Lee, Changmo Yeo, Sang-Uk Cheon, Jun Hwan Park, and Duhwan Mun. 2023. BRepGAT: Graph neural network to segment machining feature faces in a B-rep model. *Journal of Computational Design and Engineering* 10, 6 (2023), 2384–2400.
- [22] Ruoshan Lei, Hongjin Wu, and Yibing Peng. 2022. Mfpoinetnet: A point cloud-based neural network using selective downsampling layer for machining feature recognition. *Machines* 10, 12 (2022), 1165.
- [23] Guohao Li, Chenxin Xiong, Ali Thabet, and Bernard Ghanem. 2020. Deepergcn: All you need to train deeper gcns. *arXiv preprint arXiv:2006.07739* (2020).
- [24] Haiyan Li, Yunbao Huang, Yuhang Sun, and Liping Chen. 2015. Hint-based generic shape feature recognition from three-dimensional B-rep models. *Advances in Mechanical Engineering* 7, 4 (2015), 1687814015582082.
- [25] Yaolong Ma, Yingzhong Zhang, and Xiaofang Luo. 2019. Automatic recognition of machining features based on point cloud data using convolution neural networks. In *Proceedings of the 2019 international conference on artificial intelligence and computer science*. 229–235.
- [26] Fangwei Ning, Yan Shi, Maolin Cai, and Weiqing Xu. 2023. Part machining feature recognition based on a deep learning method. *Journal of Intelligent Manufacturing* 34, 2 (2023), 809–821.
- [27] Dheeraj Peddireddy, Xingyu Fu, Anirudh Shankar, Haobo Wang, Byung Gun Joung, Vaneet Aggarwal, John W Sutherland, and Martin Byung-Guk Jun. 2021. Identifying manufacturability and machining processes using deep 3D convolutional networks. *Journal of Manufacturing Processes* 64 (2021), 1336–1348.
- [28] Dheeraj Peddireddy, Xingyu Fu, Haobo Wang, Byung Gun Joung, Vaneet Aggarwal, John W Sutherland, and Martin Byung-Guk Jun. 2020. Deep learning based approach for identifying conventional machining processes from CAD data. *Procedia Manufacturing* 48 (2020), 915–925.
- [29] Charles Ruizhongtai Qi, Li Yi, Hao Su, and Leonidas J Guibas. 2017. Pointnet++: Deep hierarchical feature learning on point sets in a metric space. *Advances in neural information processing systems* 30 (2017).
- [30] Peizhi Shi, Qunfen Qi, Yuchu Qin, Paul J Scott, and Xiangqian Jiang. 2020. A novel learning-based feature recognition method using multiple sectional view representation. *Journal of Intelligent Manufacturing* 31 (2020), 1291–1309.
- [31] Yang Shi, Yicha Zhang, and Ramy Harik. 2020. Manufacturing feature recognition with a 2D convolutional neural network. *CIRP Journal of Manufacturing Science and Technology* 30 (2020), 36–57.
- [32] Jan H Vandenbrande and Aristides AG Requicha. 1993. Spatial reasoning for the automatic recognition of machinable features in solid models. *IEEE Transactions on Pattern Analysis and Machine Intelligence* 15, 12 (1993), 1269–1285.
- [33] Yue Wang, Yongbin Sun, Ziwei Liu, Sanjay E Sarma, Michael M Bronstein, and Justin M Solomon. 2019. Dynamic graph cnn for learning on point clouds. *ACM Transactions on Graphics (tog)* 38, 5 (2019), 1–12.
- [34] Tony C Woo. 1982. Feature extraction by volume decomposition. In *Proc. Conf. CAD/CAM Tech. Mech. Eng.*, Vol. 76.
- [35] Hongjin Wu, Ruoshan Lei, Yibing Peng, and Liang Gao. 2024. AAGNet: A graph neural network towards multi-task machining feature recognition. *Robotics and Computer-Integrated Manufacturing* 86 (2024), 102661.
- [36] Mingyuan Xia, Xianwen Zhao, and Xiaofeng Hu. 2024. Machining feature and topological relationship recognition based on a multi-task graph neural network. *Advanced Engineering Informatics* 62 (2024), 102721.
- [37] Keyulu Xu, Weihua Hu, Jure Leskovec, and Stefanie Jegelka. 2018. How powerful are graph neural networks? *arXiv preprint arXiv:1810.00826* (2018).
- [38] Zongyi Xu, Xiaoshui Huang, Bo Yuan, Yangfu Wang, Qianni Zhang, Weisheng Li, and Xinbo Gao. 2024. Retrieval-and-alignment based large-scale indoor point cloud semantic segmentation. *Science China Information Sciences* 67, 4 (2024), 142104.
- [39] Hongxiang Yan, Chunping Yan, Ping Yan, Yuping Hu, and Shibin Liu. 2023. Manufacturing feature recognition method based on graph and minimum non-intersection feature volume suppression. *The International Journal of Advanced Manufacturing Technology* 125, 11 (2023), 5713–5732.
- [40] Xinhua Yao, Di Wang, Tao Yu, Congcong Luan, and Jianzhong Fu. 2023. A machining feature recognition approach based on hierarchical neural network for multi-feature point cloud models. *Journal of Intelligent Manufacturing* 34, 6 (2023), 2599–2610.
- [41] Yu Zhang, Yongsheng Zhang, Kaiwen He, Dongsheng Li, Xun Xu, and Yadong Gong. 2022. Intelligent feature recognition for STEP-NC-compliant manufacturing based on artificial bee colony algorithm and back propagation neural network. *Journal of Manufacturing Systems* 62 (2022), 792–799.
- [42] Zhibo Zhang, Prakhar Jaiswal, and Rahul Rai. 2018. FeatureNet: Machining feature recognition based on 3d convolution neural network. *Computer-Aided Design* 101 (2018), 12–22.